Selection of 3 compounds able to inhibit the NLRP3 inflammasome activation in the low micro/nanomolar range endowed with drug-like properties
(D5.13 - SGA3)

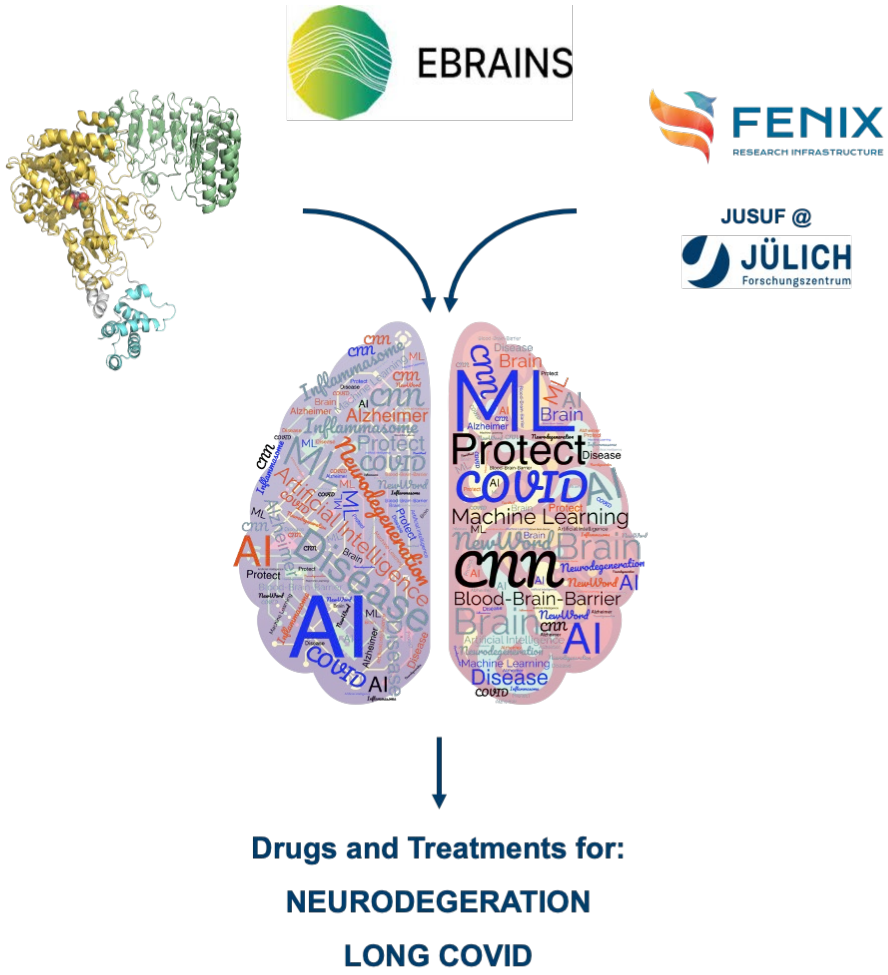

Figure 1: In silico design of NLRP3 inhibitors to target neurodegeneration.

Project Number:	945539	Project Title:	HBP SGA3

Document Title:	Selection of 3 compounds able to inhibit the NLRP3 inflammasome activation in the low micro/nanomolar range endowed with drug-like properties.
Document Filename:	D5.13 (D109) SGA3 M42 SUBMITTED 230926.docx
Deliverable Number:	SGA3 D5.13 (D109)
Deliverable Type:	Report
Dissemination Level:	PU = Public
Planned Delivery Date:	SGA3 M42 / 30 SEP 2023
Actual Delivery Date:	SGA3 M42 / 26 SEP 2023
Author(s):	Francesca SPYRAKIS, UNITO (P152)
Compiled by:	Francesca SPYRAKIS, UNITO (P152)
Contributor(s):	Giorgio COLOMBO, UNIPV (P70), contributed to Section 2.1 Massimo BERTINARIA, UNITO (P152), contributed to Section 2.3 Elisabetta MARINI, UNITO (P152), contributed to Section 2.4 Rebecca WADE, HITS (P26), contributed to Section 2.1 Giulia ROSSETTI, JUELICH (P20), contributed to Section 2.1 Paolo CARLONI, JUELICH (P20), contributed to Section 2.1
WP QC Review:	Evita MAILLI, ATHENA (P133)
WP Leader / Deputy Leader Sign Off:	Yannis IOANNIDIS, ATHENA (P133)
T7.4 QC Review:	Formatted by Annemieke MICHELS, EBRAINS (P1)
Description in GA:	The compounds identified via in silico simulations will be synthesized and tested in vitro to verify the anti-inflammatory effect. Best performing compounds will be selected according to preliminary ADME experiments. At least one compound will be identified for further in vivo studies and patenting.
Abstract:	The development of target-specific compounds that cross the Blood Brain Barrier and act as neuroinflammation inhibitors can provide fresh opportunities for the treatment of the consequences of Covid-19 infections on the brain. In a larger context, discovered molecules may act as new leads for neurodegeneration-effect treatments. Herein, starting from extensive molecular simulations to characterize the functional dynamics of NLRP3 coupled to a Machine Learning approach to select active ligands, we describe the development of a series of compounds that inhibit NLRP3-related inflammation pathways. From the series, we select 3 compounds active in the low-micromolar range and able to cross the BBB that constitute promising points for the development of novel drugs.
Keywords:	Drug discovery, Molecular Simulations, Neuroinflammation, Machine Learning, NLRP3
Target Users/Readers:	computational neuroscience community, HPC community, neuroscientific community, neuroscientists, researchers, scientific community.

Table of Contents

Table of Tables

Table of Figures

1. Introduction

The present project, BRAVE (Protecting the brain from COVID-19-mediated neurodegeneration through inflammasome inhibition), answered the HBP calls for expression of interest for SGA3 “COVID-19 and its impact on the brain and mental health”.

BRAVE focuses on the development of computational approaches, complementing and integrating EBRAINS tools and services, to advance the investigation of COVID-19-related brain disorder mechanisms into the discovery of novel drug candidates able to block SARS-CoV-2-induced excessive inflammatory responses in the brain.

The task (T5.22) which underpins the present deliverable has identified active small molecules, together with modelling their binding mode to the protein NLRP3 (the main protein effector involved in the mechanisms leading to brain disorders and neurodegeneration) and simulating their effect on NLRP3 functionally oriented dynamic properties and networks of interaction. The discovered new ligands are intended to inhibit the inflammatory response that is observed after COVID-19 infection, one of the main causes of brain disorders. Identified molecules should also have anti-inflammatory effects on neuroinflammation associated to several neurodegenerative diseases, as Alzheimer’s disease (AD) and Parkinson’s disease (PD).

Specific Objectives of the task that allowed to reach the present deliverable were i. the structural and dynamic requirements for effective drug-NLRP3 complex formation; ii. the impact of ligands on the internal dynamics of the target in terms of allosteric modulation and modification of Protein-Protein Interactions and networks; iii. the efficacy of designed ligands in vitro and their capability of crossing the BBB in vivo.

This deliverable also contributes to the HBP modelling scientific area. Indeed, to be achieved, specific computational tools have been developed and applied. Considering the development of new neuro-anti-inflammatory molecules and the mentioned tools, the following communities should be interested: computational neuroscience community, HPC community, neuroscientific community, neuroscientists, researchers, scientific community. The used tools have been shared in the KG and are available to the HBP community, and the proposed molecules represent an important starting point for the development of new anti-neurodegenerative drugs. Indeed, some of the identified molecules have been already published (P4078), while others here described will be likely submitted for patenting in the near future. The work here described thus contributes to the computing and medicine HBP downstream applications.

More specifically, we contributed to the areas of:

- modelling, structural computational biology: through the improvement of computational methods for drug design, analyses of protein dynamics, and of ligand-modulated interactions.
- chemical biology: new chemical tools from the combination of the structural methods mentioned above with drug activity studies, synthesis, and in vitro functional assays, in the context of proteins involved in inflammatory responses to pathogenic viruses.
- development of drugs against COVID-19-induced and other brain diseases: through the set-up of tools and protocols and their integration into a multidisciplinary technological platform that can be exported as a model study.

The tools used for modelling identification are the following:

- MEDIUM : https://search.kg.ebrains.eu/instances/7c3dbeb1-cb2c-4fab-910d-9fe0ca8709e9
- MLCE : https://search.kg.ebrains.eu/instances/a164f8e6-bc1a-4c17-9bb0-0dab0014b3d2
- DF : https://search.kg.ebrains.eu/instances/3647a7eb-a233-440a-8b57-87fed1ec4c01

These methodologies have expanded the umbrella of molecular tools in Task 5.17 (WP5) and their integration (in Task 5.1) in the multiscale toolset of WPO5.1 (Brain modelling and simulation), by developing tools and workflows as EBRAINS services for molecular data, either derived from experiments or from simulations, for multiscale modelling, PPI and network modelling, and simulation of neurological processes.

Calculations have been run thanks to the FENIX infrastructure (Application number 25681, computational time assigned to Francesca Spyrakis).

Chemical synthesis and in vitro testing have been performed at UNITO (P152), thanks to the collaboration with Prof. Massimo Bertinaria, Dr. Elisabetta Marini (Department of Drug Science and Technology, University of Turin) and Prof. Chiara Riganti (Department of Oncology, University of Turin).

2. Results

2.1 NLRP3: from the effects of allosteric binding to implications for drug design

2.1.1 Tools development and application

2.1.1.1 Structural organization of NLRP3

From the structural point of view, NLRP3 is organised in three main different domains: the *N*-terminal Pyrine domain (PYD), the central NACHT domain designated to accommodate ADP and the C-terminal Leucine-Rich Repeat (LRR). A flexible linker combines PYD with NACHT (**Figure 2**).

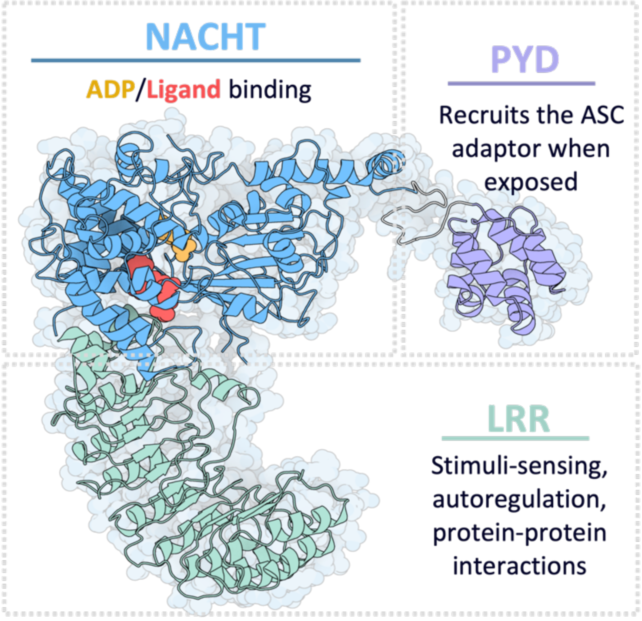

Figure 2: Structural organization of NLRP3.

2.1.1.2 NLRP3 functional dynamics and long-range coordination

The cryoEM structure of the NLRP3 monomer complexed with ADP and the MCC950 inhibitor (1-(1,2,3,5,6,7-hexahydro-s-indacen-4-yl)-3-[4-(2-oxidanylpropan-2-yl)furan-2-yl]sulfonyl-urea; PDB ID 7pzc) was used as the starting point for extensive explicit solvent, all-atom MD simulations, run on Fenix (1.365443 core-h on Jusuf CPU; 661094 core-h on Jusuf GPU). Specifically, the latter were run on NLRP3 bound to ADP (simulation labelled ADPstate) and bound to both ADP and MCC (MCCstate). The total length of the simulations for each system was 4 μs and allowed the observation of differences in the conformational stabilization of the states (Figure 3). In both states, PYD appears as the most flexible region. However, the presence of MCC induces a PYD rearrangement that makes it inaccessible for establishing interactions with other monomers in the assembly of functional NLRP3 oligomers. Altogether, these analyses show that the allosteric ligand significantly perturbs the overall dynamics of NLRP3 and favours conformational ensembles that are not poised to form the inter-monomer PYD-mediated interactions that eventually translate into the assembly of functional oligomers.

To gain more insights into the impact of MCC on the protein internal dynamics in terms of short- and long-ranged perturbations, and ultimately, on its biological function, we computed the pairwise fluctuations of residue distances in all MD trajectories, that is known to be related to the degree of coordination and allosteric communication between different protein substructures. Different motions could be associated to different protein functions. Both matrices exhibit a block character, which is typical of multidomain proteins, however finely tuned MCC-dependent modulations of NLRP3 internal dynamics can be observed. In the MCC-state, PYD loses coordination with all the remaining portions of the protein, which may favour a more disordered type of domain dynamics (Figure 4).

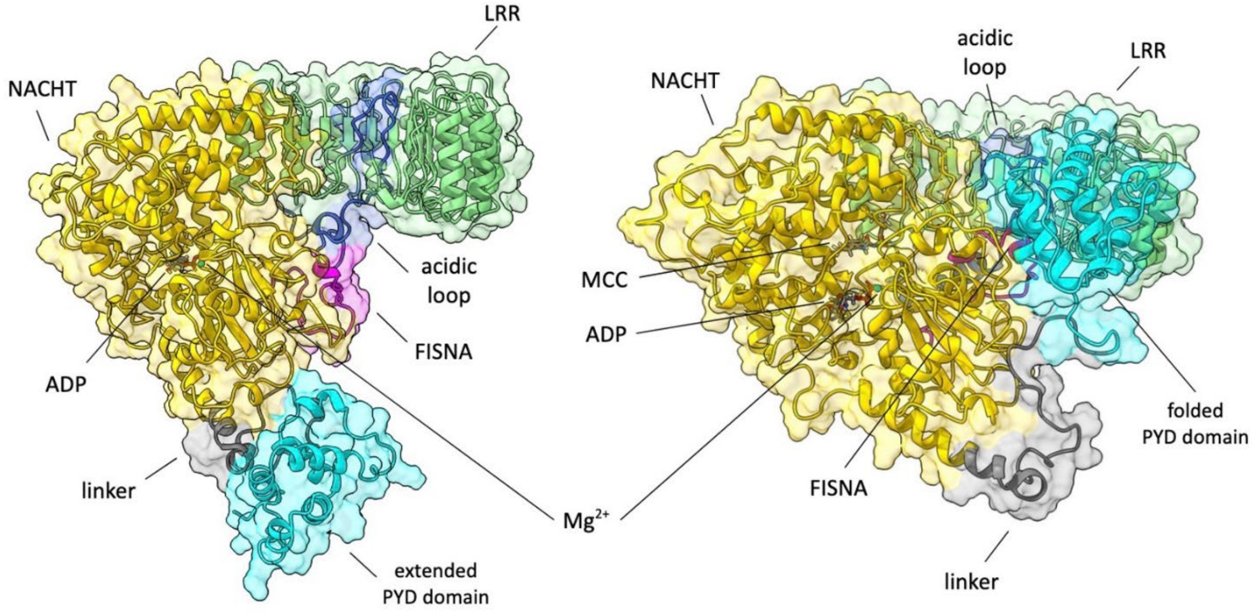

Figure 3: Representative structures of NLRP3 monomer without (left) and with (right) MCC.[1]

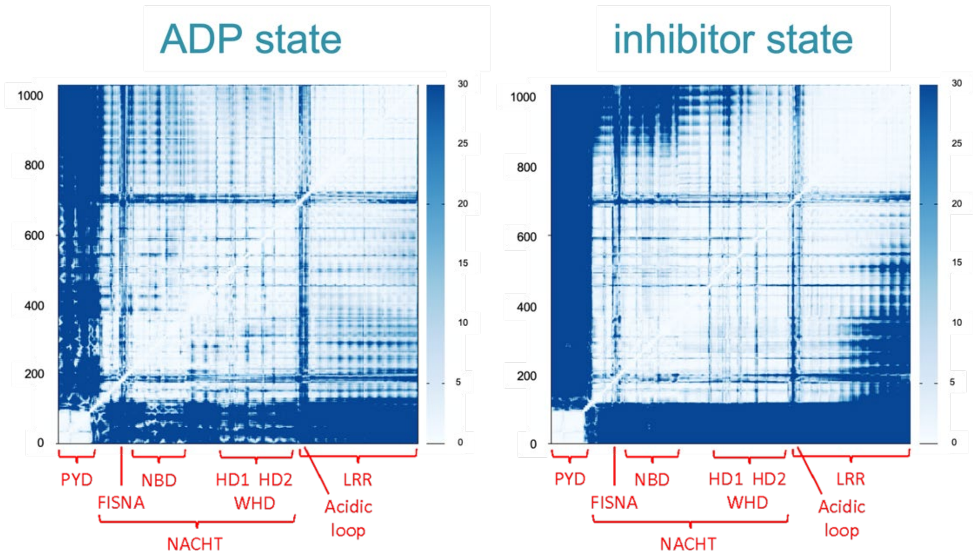

Figure 4: Distance fluctuation (DF) matrices for ADPstate and MCCstate.[1]

---

[1] Pictures taken from 10.1016/j.ijbiomac.2023.125609

2.1.1.3 Ligand effect on PPI surfaces

One of the direct computational strategies to predict protein-protein interfaces is the use of the Matrix of Low Coupling Energies (MLCE) energy decomposition method. This method is based on the concept that non-optimized, low-intensity energetic interaction networks in the protein structure may correspond to localized regions with low-intensity energetic couplings with the rest of the protein, which allows them to undergo conformational changes and work as PP recognition sites. MLCE starts by analysing the pairwise interaction energies of all amino acids in a protein.

MLCE operates in a multistep process, in which it first calculates the unbound part of the potential E (van der Waals, electrostatic interactions, solvent effects) through an MM/GBSA calculation, obtaining, for a protein of N residues, an N x N M_{ij} symmetric interaction matrix, which can be expressed in terms of eigenvalues and eigenvectors. From this point of view, we can filter the approximated interaction matrix M_{ij} so that it contains only those pairs of residues that are in geometric proximity in the analysed structure, resulting in the Matrix of the Local Coupling Energy. We select the residues involved in the 15% of non-zero interactions that are less energetic. This cut-off value proved to be a key parameter for specificity/sensitivity of the approach. The obtained residues are then fused into patches, which are sets of residues close to each other and constitute the predicted Protein-Protein Binding regions. Weaker pairwise interactions, combined with the localization of residues in continuous areas on the protein surface, highlight substructures that are not internally optimized and are therefore prone to interact with a potential partner.

Specifically, we applied MLCE to the representative structures of the most populated conformational clusters extracted from the ADPstate and MCCstate simulations. In the ADPstate, the top and front regions of the NACHT domain, highlighted in violet and red in Figure 5a, are predicted as possible interaction regions. This result is consistent with the recently published supramolecular, disk-shaped structure of polymeric NLRP3 (PDB ID 8ej4), where the most relevant monomer-monomer interface involves exactly the two substructures of the NACHT domain here predicted (i.e. interface A in Figure 5b). MLCE also defines the concave (internal) surface of LRR as a putative interaction region. Interestingly, in the above-mentioned supramolecular structure, this substructure engages in an interaction with the centrosomal kinase NEK7, which helps keep the structure open and extended.

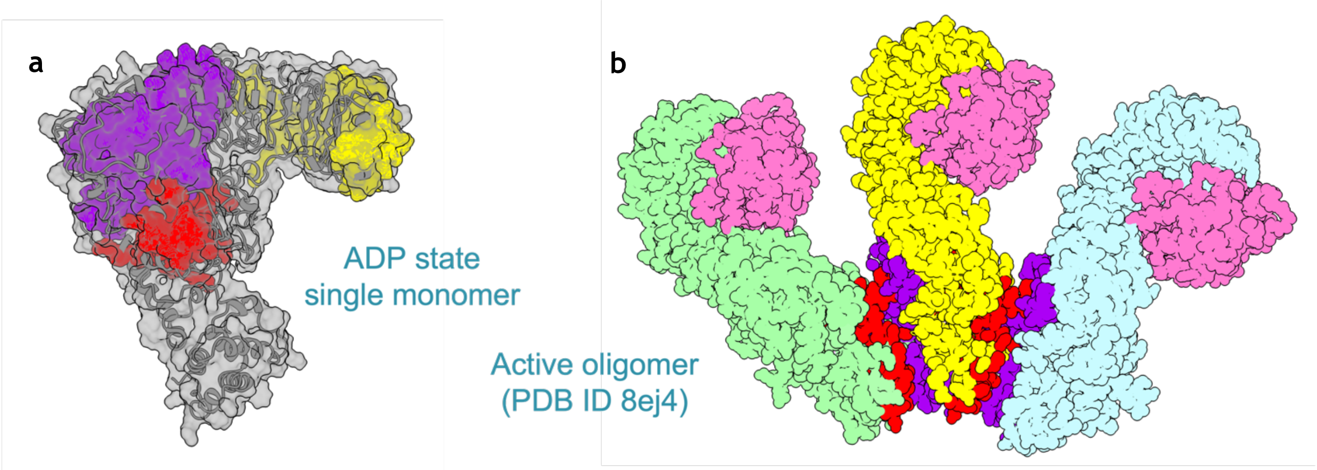

Figure 5: MCLE analysis of ADPstate.[2]

In the MCCstate, a first potential PPI interface is located on the external surface of the LRR domain (Figure 6a, orange surface), in agreement the assembly of the inactive decamer (PDB ID 7pzc), where two distinct LRRs from two consecutive monomers establish contacts through the predicted interface (Figure 6b, interface A). This result is also consistent with observations from Geyer and co-workers who implied this interaction as an important stabilising factor in the decamer assembly. The second PPI interface here predicted is located on (the external portion of) the NACHT domain, specifically involving the helices in the HD2 subdomain (Figure 6a, green surface). Importantly, in the inactive decamer, this region is involved in interactions with the terminal portion of the LRR domain and the

---

[2] Picture taken from 10.1016/j.ijbiomac.2023.125609

third and fourth helix of HD2 subdomain of two consecutive monomers (Figure 6b, interface B). Finally, MLCE returned a prediction of PPIs on the PYD domain (Figure 6a, magenta surface), which is also corroborated by the PYD-PYD interactions observed experimentally in the assembly of the inactive decamer (see Figure 6b).

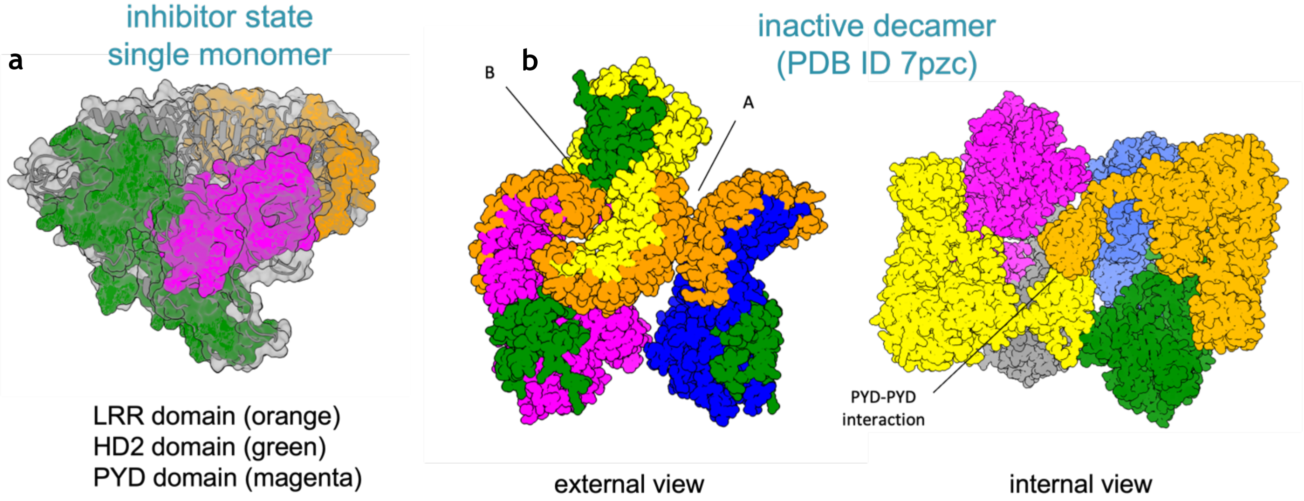

Figure 6: MCLE analysis of MCCstate.[3]

Summarising, the energy-based prediction of potential PPI interfaces indicates that different interacting substructures may emerge and be presented for partner-binding as a function of the ligand-state of the protein. In our model, the presence of MCC determines a rearrangement consistent with a model where monomers are preorganized to assemble via interactions observed in the recently described decamer form: this is achieved via the specific interaction interfaces, that present distinct structural and physico-chemical profiles from the ones observed in the ADPstate.

2.1.1.4 MD-based machine Learning Classification of active/inactive states

The results reported above provide a detailed view of the mechanisms of ligand-based regulation of NLRP3 functions, and of the impact of different ligand combinations on potential interacting surfaces. The proposed model is, in fact, able to differentiate functionally inactive dynamic states induced by the presence of MCC, from biologically active ensembles. This would allow the automatic classification of protein ligand-induced states as active or inactive, without the need for in-depth and extensive analysis of the trajectories. To meet this challenge, we further developed and tested a Machine Learning approach, called MEDIUM and available in KG (vide infra), that, starting from the analysis of images corresponding to Distance Fluctuation (DF) matrices (see above), can classify the protein as active or inactive. Indeed, DF images capture the overall state of the protein, since small modifications within the protein structural organisation (such as ligand binding or even mutation) can impact on the overall coordination propensity.

To classify the protein state as Active or Inactive, we applied Convolutional Neural Networks (CNN). Specifically, we used the VGG19 classification algorithm, directly available from Tensorflow (TF), and showing an optimal compromise between computational cost and accuracy. The detailed procedure is described in Figure 7: a) the architecture of modified VGG19 mode; b) different states of the protein involved in the study with the DF matrices (left) and performance evaluation of training and validation of the CNN ML-model (right); c) confusion matrix for the test data set using the trained ML-model.

By evaluating our trained model on the test set, we got 100% of accuracy, taking less than 1s to scan all the 42 DF test images. This result is corroborated by the confusion matrix, which perfectly showed

---

[3] Picture taken from 10.1016/j.ijbiomac.2023.125609

that amongst forty-two (42) total images, 21 test entries were correctly classified as Active while the other 21 as Inactive.

Overall, the combination of MD simulations and ML image recognition proves able to correctly classify different states of a protein, based only on the analysis of its internal dynamics. The potential of this classification method can allow us to predict the effect of other types of small molecule effectors binding in the MCC site, even with completely different structures, whose functional role is not known a priori. Given the difficulties in generating SARs for allosteric drug candidates, the use of dynamical descriptors and ML can help prioritise compounds with desired functional properties. This result is presented as a verifiable experimental hypothesis and has been used for the design novel generations of NLRP3 inhibitors.

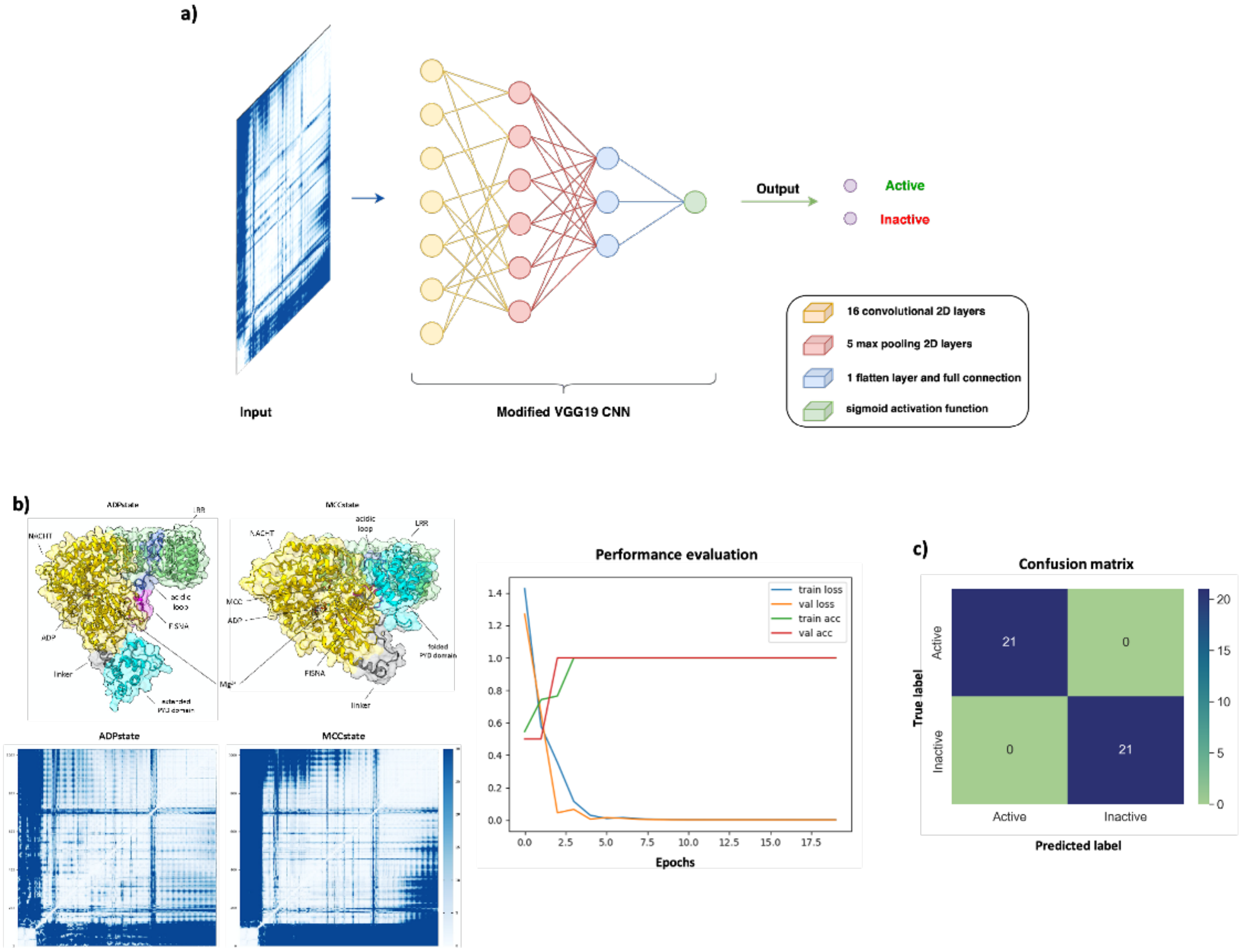

Figure 7: MEDIUM workflow.[4]

The results here presented have been published in 2023 in the International Journal of Biological Macromolecules (doi: 10.1016/j.ijbiomac.2023.125609; https://arxiv.org/abs/2309.03589; P4079; OP5.47), while the developed and applied tools are available in the KG at the following links:

- DF : https://search.kg.ebrains.eu/instances/3647a7eb-a233-440a-8b57-87fed1ec4c01
- MLCE : https://search.kg.ebrains.eu/instances/a164f8e6-bc1a-4c17-9bb0-0dab0014b3d2
- MEDIUM : https://search.kg.ebrains.eu/instances/7c3dbeb1-cb2c-4fab-910d-9fe0ca8709e9

These tools are also available in the EBRAINS molecular and subcellular level simulation tool suite at https://www.ebrains.eu/modelling-simulation-and-computing/simulation/molecular-and-subcellular-simulation.

---

[4] Picture taken from 10.1016/j.ijbiomac.2023.125609

2.2 Identification of the structural requirement a molecule should have to target NLRP3

2.2.1 Identification of key moieties in NLRP3 inhibitors

In the last decade, the investigation for NLRP3 inhibitors became of great interest in academia and industry, leading to the discovery of both reversible and covalent NLRP3 inhibitors. Different chemical scaffolds have been used to design NLRP3 inhibitors, the most effective up to now being di-substituted sulfonylurea typical of glyburide. Notable examples are MCC950 (also known as CRID3) and NP3-146 (Figure 8A and 8B, respectively). Sulfonylurea-based inhibitors bind to an allosteric pocket in the NACHT domain of NLRP3, at the interface of HD1, HD2, NBD, FISNA and WHD subdomains and adjacent to the nucleotide binding site, as shown in Figure 8C. This allosteric pocket is shaped by residues belonging to different subdomains of the NACHT domain and is only apparent in the inactive, ADP-bound conformation. Indeed, a recently published cryo-EM structure shows that, upon activation, HD1, HD2, NBD, FISNA and WHD subdomains undergo a massive conformational change, which requires a 85.4° rigid body rotation of the FISNA-NBD-HD1 module with respect to the WHD-HD2-LRR module, on an axis located between subdomains HD1 and WHD (Figure 8D). Therefore, in the active, ATP-bound form of NLRP3, the allosteric pocket cannot be detected. The inhibitory activity of sulfonylurea-based inhibitors derives from their ability to glue together the HD1, HD2, NBD and WHD subdomains constituting the allosteric pocket, eventually avoiding the activation of NLRP3 NACHT domain.

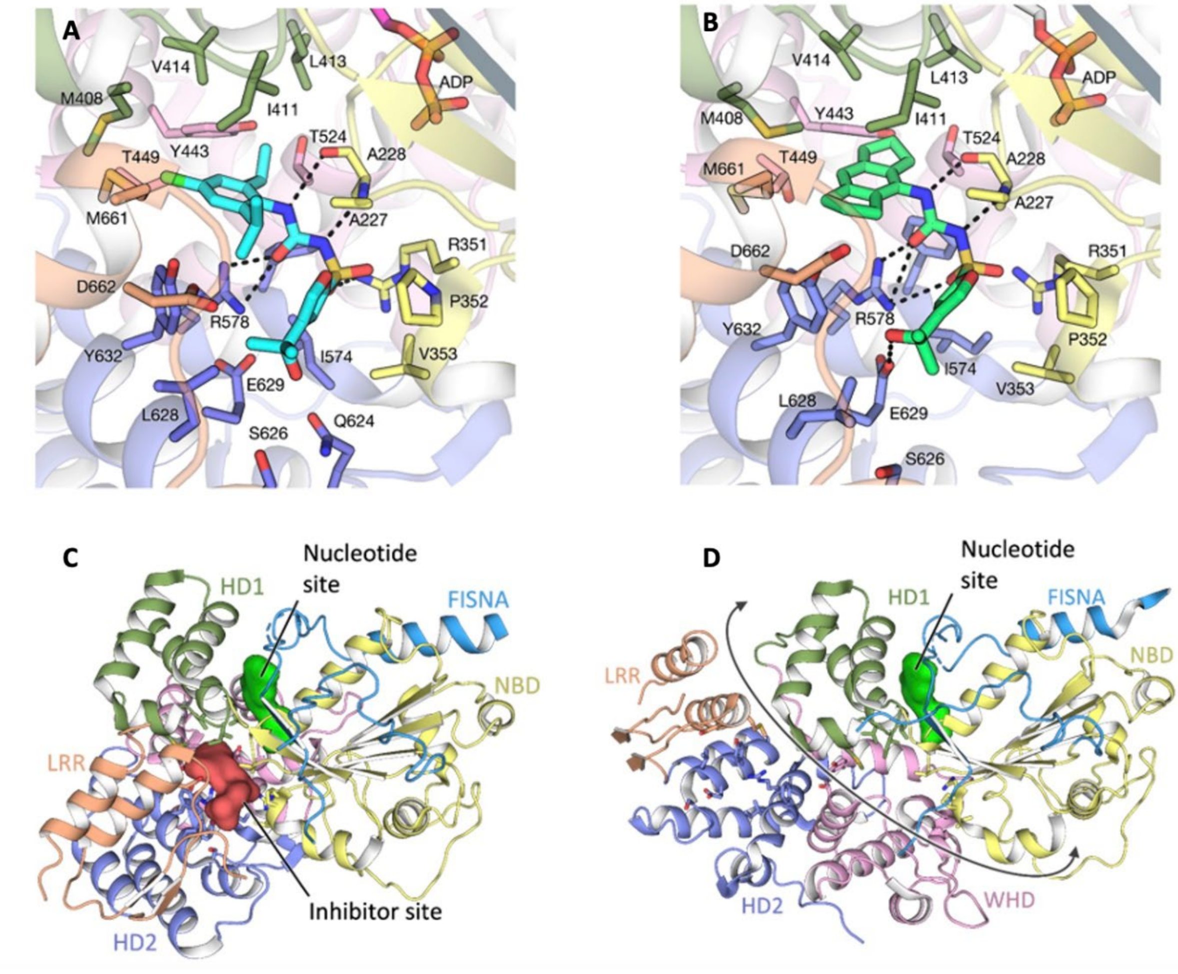

Figure 8: Structural information on NLRP3 active/inactive state.[5]

---

[5] Picture taken from 10.1016/j.ejmech.2023.115542

2.2.2 *Design of new NLRP3 inhibitor series*

Based on our previous experience in the development of NLRP3 inhibitors, we explored the possibility of designing new non-sulfonylurea based NLRP3 inhibitors. The interaction of the latter with NLRP3 can be generally schematized in three blocks (Figure 9): (i) the lipophilic tail, represented by the *s*-hexaydroindacene in MCC950 or the 4-chloro-2,6-diisopropylbenzene ring in NP3-146 that fits into a hydrophobic pocket; (ii) the sulfonylurea moiety establishes a network of hydrogen bonds with Ala228 and Arg578 of the HD2 subdomain; (iii) the sulfonamide oxygen binds to the positively charged Arg351 of the NBD subdomain. The terminal substituted furanyl moiety in MCC950 is not essential as it has been extensively modulated by using either aromatic and heteroaromatic rings appropriately substituted to improve physicochemical and pharmacokinetic properties of this class of compounds.

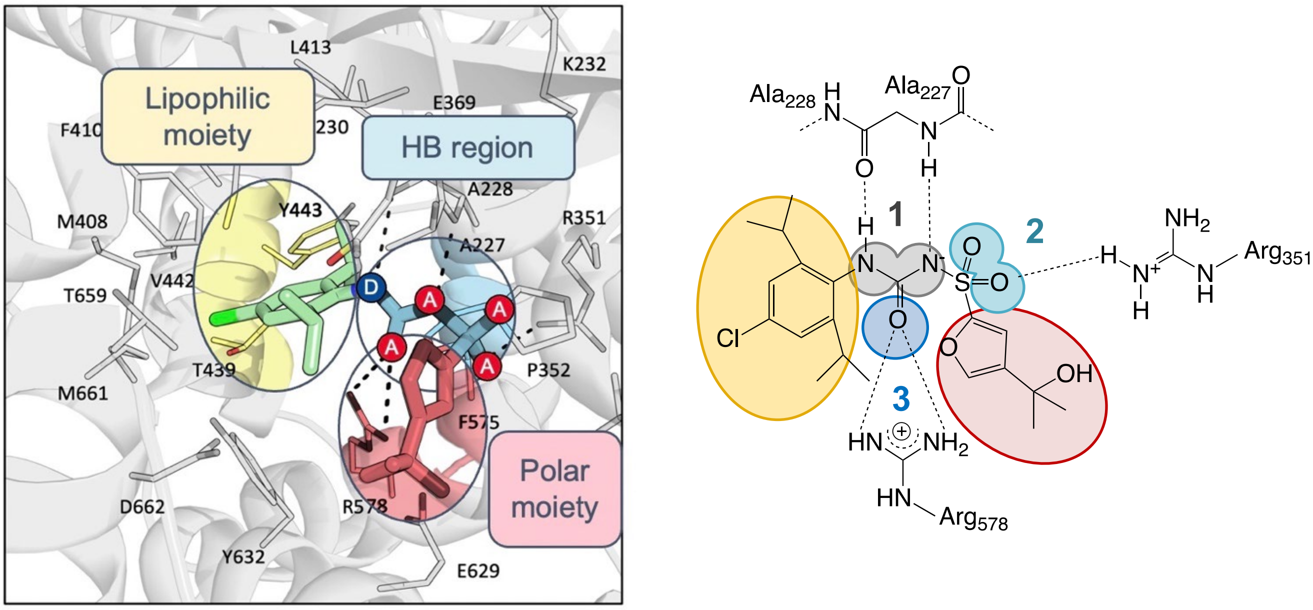

Figure 9: 3D and schematic view of NLRP3 inhibitor moieties.

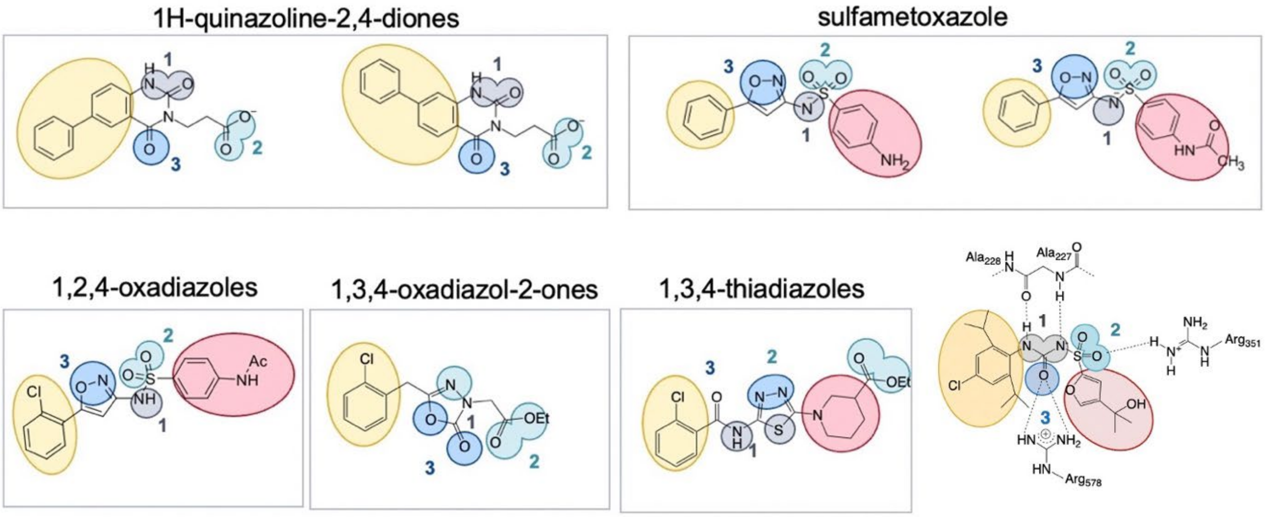
1H-quinazoline-2,4-diones

sulfametoxazole

1,2,4-oxadiazoles

1,3,4-oxadiazol-2-ones

1,3,4-thiadiazoles

Figure 10: Representative compounds of the synthesized series.

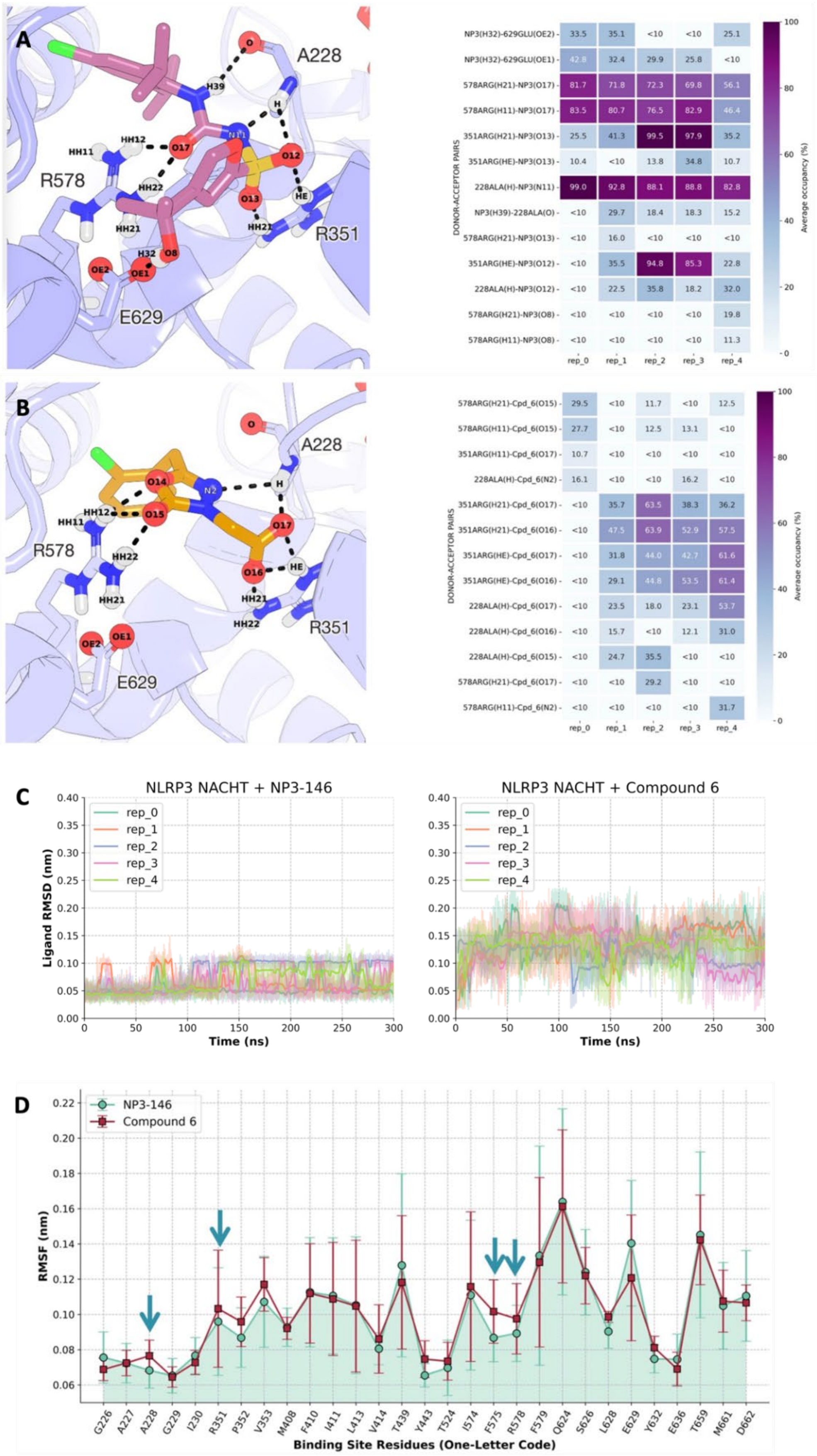

Figure 11: Example of NLRP3-ligand MD trajectory analysis for compound INF200.[6]

---

[6] Picture taken from 10.1016/j.ejmech.2023.115542

We have maintained the three mentioned key blocks of interactions by replacing the sulfonylurea-based central core with different heterocycles, while performing limited structural modulations to the lipophilic moiety and terminal polar group. In particular, we used a substituted benzene ring as the lipophilic moiety and a carboxylic acid functionality, or its ester prodrug, as polar group (Figure 10), and linked the three blocks using spacers endowed with different size and flexibility. The spacer chemical nature and length were varied to maintain the interaction with Arg351, as its flexibility can be hardly predicted. The synthetic accessibility of the differently substituted heterocycles was also considered in the design of new compounds.

Different series, trying to resemble the main interaction previously described have been designed, modelled, synthesized, and tested. Modelling simulations, performed by means of molecular docking, molecular dynamics, DF, MLCE and MEDIUM analyses, have guided the selection of the most promising compounds to be synthesized. In Figure 10 some of the representative of the series, along with the reference NP3 compounds and the moieties involved in key interactions with the target are reported and labelled.

More specifically, and as an example, the persistence of key hydrogen bonds between the compounds and the target has been tracked during 200ns-long MD simulations and compared with the reference NP3 ligand (Figure 11A,B). The RMSD of the ligand and of the residues lining the pocket (Figure 11C,D) has been also calculated, as an average, to verify the stability of our newly designed compounds, again with respect to NP3 ligand. Moreover, the capability of the compounds to stabilize an inactive state of NLRP3, and inhibit its activation, has been tested by means of DF and MEDIUM analysis.

In the reported example (Figure 11), it is quite clear how compound INF200 is involved in less stable interactions with the NLRP3 target, with respect to the known active NP3 ligand.

Based on the mentioned analyses, in collaboration with Prof. Massimo Bertinaria (Department of Drug Science and Technology, UNITO), we synthesized and tested the compounds reported in Tables 1 and 2.

2.3 Selection of the best performing molecules

The synthesized compounds were characterized for their ability to inhibit NLRP3-dependent pyroptosis and IL-1ß release in human differentiated THP-1 and mouse J774.A.1 macrophages, upon inflammasome priming and activation.

Table 1: Newly synthesized compounds tested on J774.1 cells.

Compound ID	IC_{50} ± SEM (µM) determined on J774A.1 cells
INF229	11.8 ± 1.2
INF243	15.8 ± 4.2
INF244	9.5 ± 1.4
INF245	14.6 ± 1.8
INF246	11.1 ± 1.2
INF247	18.6 ± 3.6
INF234	10.3 ± 1.2
INF236	11.7 ± 1.3
INF237	18.2 ± 2.7
INF240	15.6 ± 2.1
INF241	13.1 ± 3.1
INF242	11.6 ± 1.2
INF238	19.5 ± 4.2
INF239	18.7 ± 1.6

Specifically, compounds reported in Table 1 were tested in J774.A.1 ($1*10^5$ cells/well in a 96-well plate). Cells were first treated with 1 µg/ml LPS to prime the inflammasome for 6 hours, and then treated with different inhibitor concentrations (1 nM, 10nM, 50 nM, 100 nM, 500 nM, 1 µM, 2.5 µM, 5 µM, 10 µM, 20 µM) for 30 minutes. 10 µM Nigericin was administered to the cells to activate the inflammasome. Measurement of IL-1β release was carried out after 1 hour by means of an ELISA assay, and IC$_{50}$ was determined.

The following series (Table 2), recently published in (doi 10.1016/j.ejmech.2023.115542; P4078; OP5.48) was evaluated in THP-1 cells for pyroptosis and IL-1β release inhibition. Briefly, THP-1 cells were plated and differentiated into macrophages by treatment with phorbol myristate acetate (PMA; 50 nM; 24 h). Differentiated cells were primed with lipopolysaccharide (LPS; 10 µg/mL; 4 h) in serum-free medium and then treated with either vehicle alone or test compound (10 µM; 1 h). The cell death was triggered with ATP (5 mM), and the pyroptotic cell death evaluated after 1.5 h by measuring the LDH released in the cell supernatants. For those compounds showing > 25 % inhibition of pyroptotic cell death at 10 µM, the % inhibition of IL-1β release in THP-1 or J774A-1 cells was evaluated via an ELISA assay (Table 2). Finally, the cytotoxicity exerted by test compounds over 72 h was evaluated using the MTT assay after treatment of THP-1 cells with increasing concentration of test compounds (0-1 – 100 µM).

Table 2: Newly synthesized compounds tested on THP-1 cells.

Compound ID	Compound structure	Pyroptosis inhibition percentage	IL-1β release inhibition percentage at 10 µM
INF198	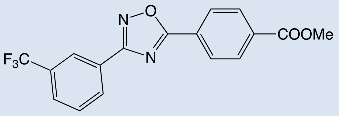	46.3 ± 17.3	<10
INF206	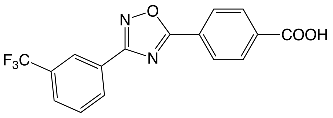	14.2 ± 2.1	NT
INF209	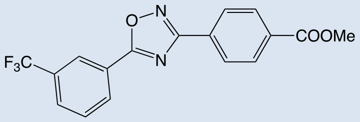	<10	NT
INF209c	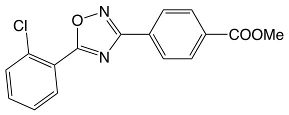	<10	NT
INF200	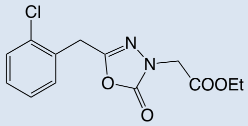	66.3 ± 6.6	35.5 ± 8.1 (16.6 ± 2.6) [a]
INF204	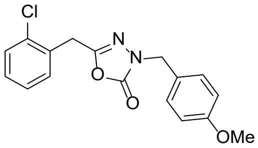	11.4 ± 3.8	NT
INF207	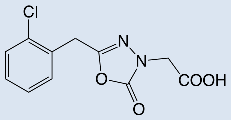	45.9 ± 8.4	30.3 ± 14.6 (32.6 ± 5.0) [a]
INF208	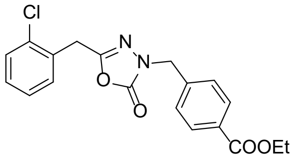	17.7 ± 6.4	NT

INF218	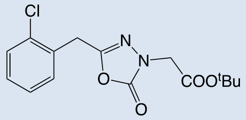	<10	NT
INF227	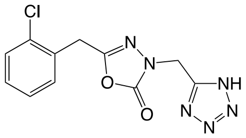	27.6 ± 9.5	<10
INF211	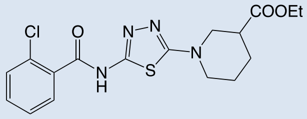	39.7 ± 13.3	22.4 ± 9.5
INF212	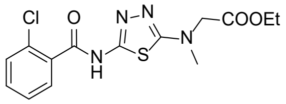	25.7 ± 5.8	20.7 ± 12.6
INF216	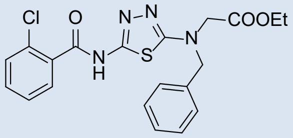	60.0 ± 13.2	49.0 ± 12.4

[a] IL-1β release IC_{50}.

Most of the selected molecules demonstrated to inhibit IL-1β release in the low micromolar range. According to *in vitro* data, *in silico* evaluation, novelty of the compounds and synthetic feasibility, three compounds (Table 3) have been selected for further characterization, in particular for BBB permeation and intestinal absorption.

2.4 BBB permeation and intestinal absorption experiments

2.4.1 *BBB permeation experiments*

Table 3: Compounds selected for BBB and intestinal permeation studies.

Compound ID	IC_{50} ± SEM (μM) determined on J774A.1 cells
INF245	14.6 ± 1.8
INF246	11.1 ± 1.2
INF234	10.3 ± 1.2

First, sulfamethoxazole-based derivatives, INF245 and INF246, have been tested. Compounds were administered i.v. to male wistar rats (250-300 g), 2.5 mg/kg.

At each time point (30, 60 and 180 minutes):

- blood was collected via transcardiac puncture, centrifuged and plasma was analysed by HPLC;
- after trans cardiac perfusion with PBS, brain was removed, homogenized, and analysed by UPLC-MS.

When INF245 is administered, it is possible to observe in plasma a certain, even if minimum, amount of INF246, likely because of INF245 being partially deacetylated in the liver (Figure 12), since INF245 is stable in rat plasma (in vitro enzymatic stability).

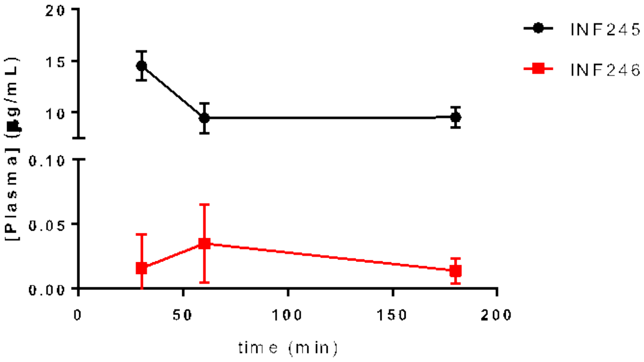

Figure 12: Plasma concentration of INF245 and INF246 upon administration of INF245.

Analysis of brain samples obtained from rats treated with INF245 did not reveal the presence of the compound, thus ruling out the possibility of INF245 exceeding the BBB in detectable quantities, this might be due to an active transporter taking INF246, but not INF245, through the BBB (Table 4).

Table 4: BBB permeation data for INF245.

District	Time (min)	µg/g tissue ± SE		µg/mL ± SE		AUC$_{0-3}$ (µg/mL.min)	K$_p$^{a}
		INF245	INF246	INF245	INF246		
Brain	30	0	0			--	--
	60	0	0				
	180	0	0				
Plasma	30			15 ± 1	0.016 ± 0.015	1503	
	60			9.5 ± 0.8	0.035 ± 0.018		
	180			9.5 ± 0.6	0.014 ± 0.005		

^{a}AUC$_{brain}$ to AUC$_{plasma}$ ratio

Similarly, INF246, the deacetylated form of INF245, has been administered to male wistar rats. Brain samples showed the presence of the compound at all tested times, with a maximum permeation at 60 minutes. At 30 minutes only INF246 has been detected, while at 60 minutes also INF245 has been detected, thus suggesting that part of the compound is transformed in the acetylated derivative, i.e. INF245 (Figure 13, Table 5). At time 180 min, most of the compound has been cleared from the brain, and only a small amount of it is detectable. Apart from the same INF246, no other metabolites were found in the plasma (Figure 13, Table 5).

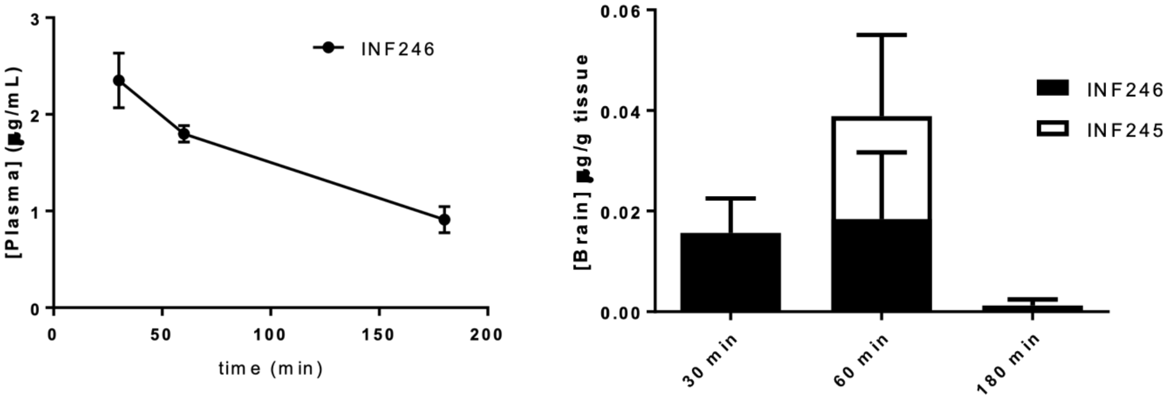

Figure 13: Plasma and brain concentration of INF246.

Table 5: BBB permeation data for INF246.

District	Time (min)	µg/g tissue ± SE		µg/mL ± SE		AUC$_{0-3}$ (µg/mL.min)	K_p
		INF246	INF245	INF246	INF245		
Brain	30	0.016 ± 0.007	0			4.84	0.022
	60	0.012 ± 0.010	0.039 ± 0.016				
	180	0.0012 ± 0.0012	0				
Plasma	30			2.4 ± 0.2	0	225	
	60			1.8 ± 0.05	0		
	180			0.91 ± 79	0.08		

Then, also INF234, belonging to the class of quinazoline compounds, showing promising in vitro values, was tested for BBB permeation, following the protocol previously described. INF235, the hydrolysed derivative of INF234 was the only compound detected at 180 minutes after administration. Considering INF234 is transformed in INF235 already in the plasma, it is quite reasonable that INF235 directly passes the BBB and reach the brain (Table 6).

Table 6: BBB permeation data for INF234.

District	Time (min)	µg/g tissue ± SE		µg/mL ± SE		AUC$_{0-3}$ (µg/mL.min)	K_p
		INF234	INF235	INF234	INF235		
Brain	180	0	0.070 ± 0.030			--	--
Plasma	180			0	0.035 ± 0.17		

2.4.2 *Intestinal permeation experiments*

The three mentioned compounds have been also tested for intestinal permeation (Figure 14, Table 7).

Each compound (5 mg/Kg: 1.5 mg/0.2 mL BPS + Methocel 3%) was syringed into intestinal sacs from different segments of rat intestine and incubated in oxygenated Krebs-Ringer buffer at 37°C with smooth shaking. Sample solution was then withdrawn from serosal side at fixed time intervals (0-2h) and replaced with fresh buffer. Samples were analysed by HPLC. At the end of permeation experiments, intestinal sacs filled with the tested compound were emptied and washed with Krebs-Ringer buffer. Tissues were homogenized and analysed by HPLC.

The experiments of intestinal permeation show that compounds (Figure 14, Table 7) are very poorly absorbed by intestinal epithelium, and they accumulate in intestinal tissues in a small extent, with no significant differences between the three intestinal sections. Specific formulations would be required to improve intestinal absorption.

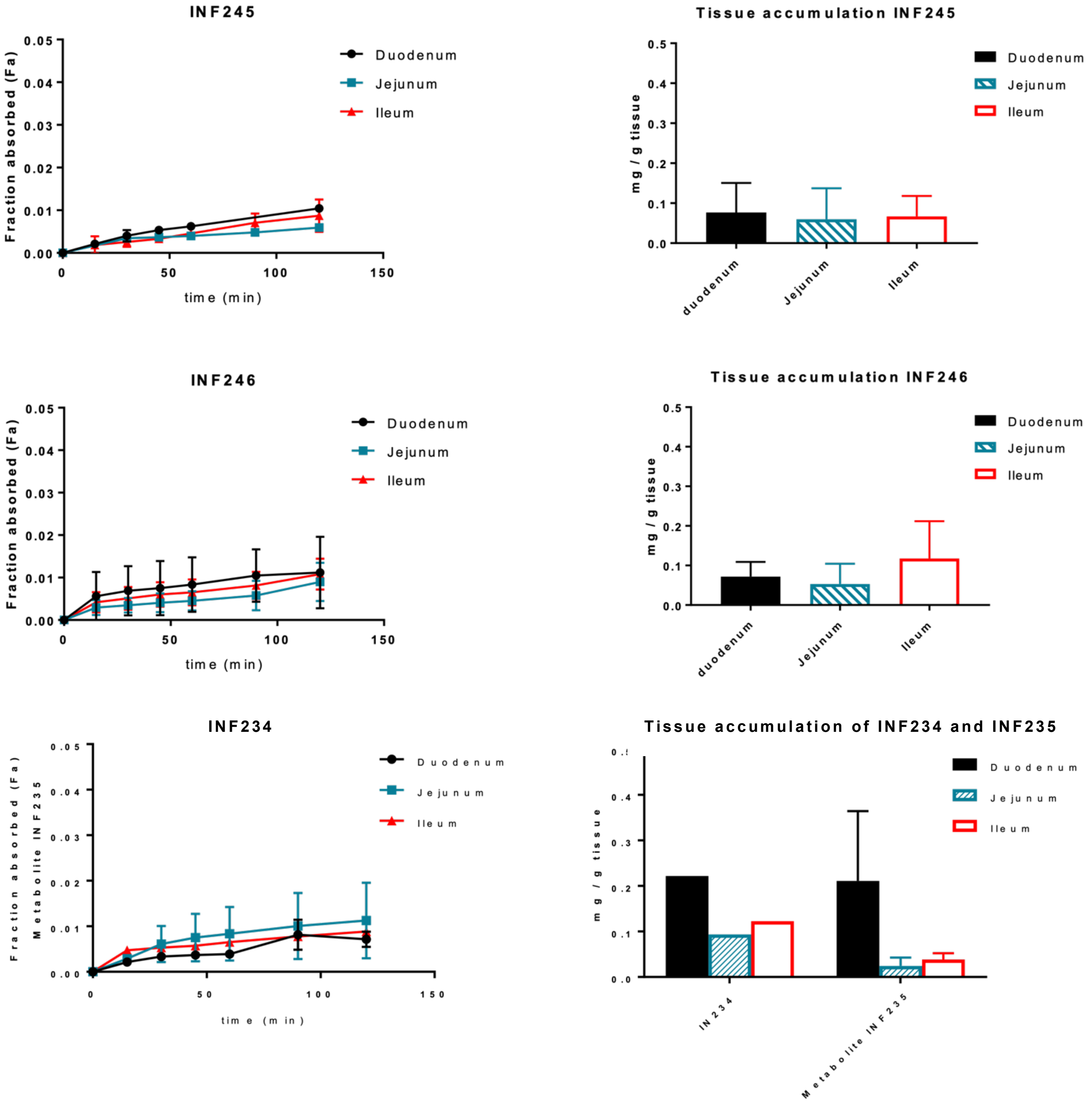

Figure 14: Absorbed fraction (left) and tissue accumulation (right) of tested compounds.

Table 7: Intestinal permeation of the tested compounds.

Compound ID	Fraction absorbed (Fa) ± SE (mg absorbed/mg dose)		
	Duodenum	Jejunum	Ileum
INF245	0.0080 ± 0.002	0.0039 ± 0.0020	0.0063 ± 0.002
INF246	0.011 ± 0.005	0.0090 ± 0.003	0.010 ± 0.002
INF234	0	0	0
	Metabolite (INF235) 0.0072 ± 0.0012	Metabolite (INF235) 0.011 ± 0.006	Metabolite (INF235) 0.0088 ± 0.0002

3. Looking Forward

The compounds that proved their capability of crossing the BBB, representing good leads for developing new treatments to target neurodegeneration, will be submitted to the following analyses:

- Check of IL-1ß release from LPS/flagellin- and LPS-poly-dA:dT-stimulated J774A.1 to prove compound selectivity for NLRP3 vs AIM2 and NLRC4 inflammasome;
- Test compounds in N11 microglia and human THP-1-derived macrophages;
- test compound cytotoxicity (MTT) in J774A.1 and another cell line (non-immune system), e.g. HEK293, HK-2 or others.

At the same time, chemical modulation of the leads is ongoing to improve the compound potency and have more room to improve ADME properties via substituent modification and/or addition. Specifically, lipophilic substitutions on the hydrophobic ring are under investigation to better fill the hydrophobic. All compounds will be submitted to DF, MCLE and MEDIUM analyses, to confirm their capability of disrupting the NLRP3 inflammasome activation.

The optimized compounds will be patented and will, likely, constitute good candidates for the development of new drugs to target neuroinflammation causing long-COVID detrimental effects and other neurodegenerative pathologies as AD and PD.